Astronomy & Astrophysics manuscript no. cr˙bergemann˙r˙ap
June 3, 2010

Chromium: NLTE abundances in metal-poor stars and nucleosynthesis in the Galaxy

M. Bergemann[1⋆] and G. Cescutti[2⋆⋆]

[1]Max-Planck Institute for Astrophysics, Karl-Schwarzschild Str. 1, 85741, Garching, Germany
[2]Astronomy Unit, Department of Physics, University of Trieste, via G.B. Tiepolo 11, I-34143, Trieste, Italy

Received date / Accepted date

ABSTRACT

Aims. We investigate statistical equilibrium of Cr in the atmospheres of late-type stars to show whether the systematic abundance discrepancy between Cr I and Cr II lines, as often encountered in the literature, is due to deviations from LTE. Furthermore, we attempt to interpret the NLTE trend of [Cr/Fe] with [Fe/H] using chemical evolution models for the solar neighborhood.

Methods. NLTE calculations are performed for the model of Cr atom, comprising 340 levels and 6806 transitions in total. We make use of the quantum-mechanical photoionization cross-sections of Nahar (2009) and investigate sensitivity of the model to uncertain cross-sections for H I collisions. NLTE line formation is performed for the MAFAGS-ODF model atmospheres of the Sun and 10 metal-poor stars with $-3.2 <$ [Fe/H] < -0.5, and abundances of Cr are derived by comparison of the synthetic and observed flux spectra.

Results. We achieve good ionization equilibrium of Cr for the models with different stellar parameters, if inelastic collisions with H I atoms are neglected. The solar NLTE abundance based on Cr I lines is 5.74 dex with $\sigma = 0.05$ dex; it is ~ 0.1 higher than the LTE abundance. For the metal-poor stars, the NLTE abundance corrections to Cr I lines range from +0.3 to +0.5 dex. The resulting [Cr/Fe] ratio is roughly solar for the range of metallicities analyzed here, which is consistent with current views on production of these iron peak elements in supernovae.

Conclusions. The tendency of Cr to become deficient with respect to Fe in metal-poor stars is an artifact due to neglect of NLTE effects in the line formation of Cr I, and it has no relation to peculiar physical conditions in the Galactic ISM or deficiencies of nucleosynthesis theory.

Key words. Line: formation – Line: profiles – Sun: abundances – Stars: abundances – Nuclear reactions, nucleosynthesis, abundances – Galaxy: evolution

1. Introduction

Abundance of chemical elements in the atmospheres of late-type stars is a key information in studies of Galactic chemical evolution (GCE). Combinations of different elements and variation of their abundances with metallicity are commonly used to calibrate GCE models and to constrain poorly-known parameters, like star formation history, initial mass function, and efficiency of mixing in the ISM. Since stellar yields are also a part of such models, the abundances can also probe the theories of stellar nucleosynthesis and evolution and highlight problems in them.

The abundances are derived by means of high-resolution spectroscopy that implies modelling the observed stellar spectrum. Whereas a poor quality of a spectrum introduces some random noise about a true value of the abundance, major *systematic* errors result from an oversimplified treatment of radiation transfer and convection in stellar atmospheres (Asplund 2005). The assumption of local thermodynamic equilibrium (LTE), which is traditionally used to compute a spectrum in an attempt to avoid numerical difficulties with line formation, breaks down for the many species. Minority ions, which constitute at most few percent of the total element abundance, are particularly affected by NLTE conditions. As a consequence, various abundance indicators of the same element, like lines of different ionization stages or excitation potentials, often give discrepant results in 1D LTE analysis. The main concern is that once observations compel us to restrict the analysis to a *single indicator*, e.g. due to a moderate signal-to-noise ratio or limited spectral range, spurious abundance trends with metallicity are unavoidable.

For Cr, even-*Z* element of the Fe-group, only LTE calculations have been performed up to now. They revealed severe problems with modelling excitation and ionisation balance of Cr in the atmospheres of late-type stars. Systematic differences of 0.1 – 0.5 dex between abundances based on LTE fitting of the Cr I and Cr II lines were reported for metal-poor giants and dwarfs (Johnson 2002; Gratton et al. 2003; Lai et al. 2008; Bonifacio et al. 2009). The discrepancies are smaller in the atmospheres with larger metal content, amounting to ~ 0.1 dex for Galactic disk stars (Prochaska et al. 2000) and for the Sun (Sobeck et al. 2007; Asplund et al. 2009). Following

⋆ E-mail: mbergema@mpa-garching.mpg.de
⋆⋆ E-mail: cescutti@oats.inaf.it

Gratton & Sneden (1991), these offsets are usually attributed to the overionization of Cr I, a typical NLTE phenomenon affecting minority atoms in stellar atmospheres. Alternatively, Bai et al. (2004) suggested uneven distribution of neutral and ionized Cr in different atmospheric layers, which depends on stellar parameters.

As a result, two views on the evolution of Cr abundances in the Galaxy exist in the literature. The constant [Cr/Fe] with metallicity is derived from the LTE analysis of Cr II lines (Gratton & Sneden 1991; Bonifacio et al. 2009) that has a simple interpretation in the theory of nucleosynthesis. Cr is formed with Fe in explosive Si-burning that occurs in supernova (SN) events, and the production ratio Cr/Fe is roughly solar in both SNe II and SNe Ia (Clayton 2003). Thus, using standard prescriptions for Cr nucleosynthesis, most of the GCE models reproduce the flat [Cr/Fe] trend with [Fe/H] (e.g. Timmes et al. 1995; Samland 1998; Goswami & Prantzos 2000).

On the other hand, most LTE analysis of Cr I lines (McWilliam et al. 1995; Cayrel et al. 2004; Cohen et al. 2004) indicate that the [Cr/Fe] ratio steadily declines towards lowest metallicity. There is no simple explanation to this trend. Some chemical evolution studies tried to overcome the problem by introducing correction factors to the theoretical SN yields (François et al. 2004; Henry et al. 2010). The assumption of erroneous supernova yields is not unrealistic, given their sensitivity to the details of explosion (Iwamoto et al. 1999; Nakamura et al. 1999). However, to reproduce an approximate trend given by spectroscopic data arbitrary scaling factors to stellar yields are usually chosen, which lack any physical justification. Also, recent studies of metal-free massive stars and their nucleosynthesis yields demonstrate that subsolar Cr/Fe abundance ratios in very metal-poor stars can not be reproduced by any combination of SN II model parameters (Umeda & Nomoto 2005; Heger & Woosley 2008), especially when other Fe-peak elements are taken into account.

In this paper, we report NLTE abundances of Cr for the Sun and a sample of dwarfs and subgiants with $-3.2 \leq$ [Fe/H] ≤ -0.5. The atomic model for Cr and details about NLTE calculations are documented in Sect. 2. The statistical equilibrium of Cr under restriction of different stellar parameters in discussed in Sect. 3. In Sect. 4, we present the NLTE analysis of solar Cr I and Cr II lines and derive the solar Cr abundance. In Sect. 5, we describe observed spectra, stellar parameters, and present Cr abundances for a sample of metal-poor stars. Finally, in Sect. 6, the revised abundance ratios [Cr/Fe] are compared with the trends predicted by GCE models and some implications for the evolution of Cr in the Galaxy are discussed.

2. The methods

2.1. Statistical equilibrium calculations

Restricted NLTE calculations for Cr are performed with the code DETAIL (Butler & Giddings 1985). In the more recent version of the code, radiative transfer is based on the method of accelerated lambda iteration.

The reference atomic model is constructed with 114 levels for Cr I and 225 levels for Cr II, with energies of 0.01 eV and 1.1 eV below the respective ionization limits, 6.77 eV and 16.49 eV. The model is closed by the Cr III ground state. The typical separation of fine structure components in Cr I and Cr II is less than 0.1 eV. Hence, we do not include fine structure in statistical equilibrium (SE) calculations. Each term is represented by a single level with a total statistical weight of the term and energy weighted by statistical weights of fine structure components. Transitions are grouped. All transitions with oscillator strengths $\log gf \leq -8$ and wavelengths $\lambda \geq 20000$ Å are neglected. As a result, the number of radiatively-allowed transitions is limited to 1590 and 5216 for Cr I and Cr II, respectively. Level excitation energies and oscillator strengths were taken from the Kurucz online database[1], supplemented by the experimental data of Murray (1992). The Grotrian diagram of the Cr I model atom is shown in Fig. 1. The atomic data for some levels, including excitation energies E_{exc}, wavelengths λ_{thr} and cross-sections σ_{thr} at ionization thresholds, are given in Table 1.

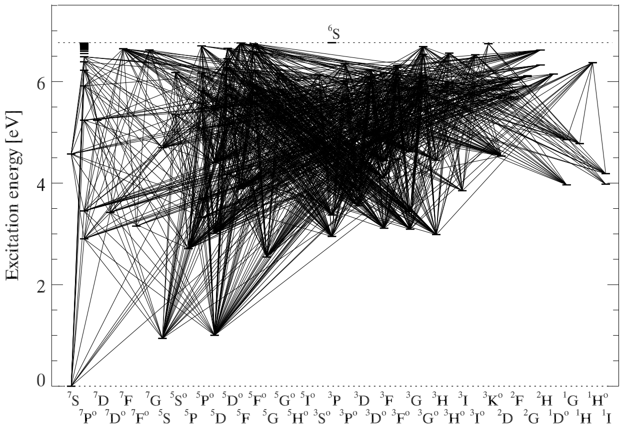

Fig. 1. Grotrian diagram of the Cr I model atom. Lines represent allowed transitions included in the model atom.

The following atomic processes are taken into account in calculations of transition rates: radiative bound-bound and bound-free transitions, excitation and ionization by collisions with free electrons, and neutral hydrogen atoms. Scattering processes follow complete frequency redistribution. Recent calculations of photoionization from quintet and septet states of Cr I (Nahar 2009) revealed resonances in cross-sections, which are due to the photoexcitation of the core leading to autoionization. The proper treatment of the latter process, e.g. transitions to autoionizing states and ionization into excited core states, is not yet possible with the DETAIL code. Thus, we used partial cross-sections for ionization into the ground state of Cr II, which are lower than the total cross-sections at energies above the first excited state of the core, $\lambda \leq 1500$ Å. This is a reasonable approximation for cool stellar atmospheres, because temperatures are lower than those needed for core excitation. We have also shifted the cross-sections to the ob-

[1] http://kurucz.harvard.edu/

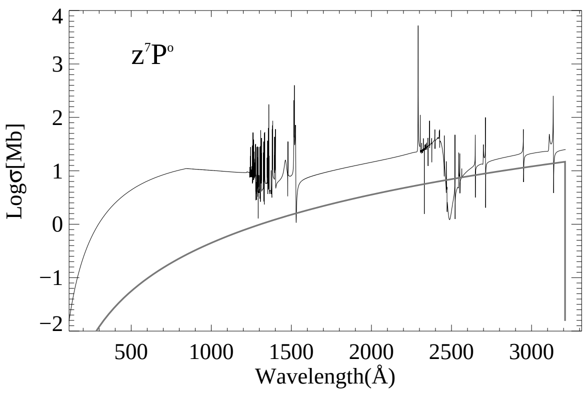

Fig. 2. Photoionization cross-section for the $z\,^7\mathrm{P}^\circ$ state of Cr I: (black trace) quantum-mechanical calculations of Nahar (2009), (gray trace) hydrogenic approximation with effective principle quantum number $n^* = 1.88$.

served edge energies of Cr I states from the NIST[2] database, because the latter are more accurate than the calculated LS term energies from Nahar (2009). Photoionization from the other Cr I and Cr II states is computed with a formula of Kramer (Menzel & Pekeris 1935) corrected for the ion charge (Rutten 2003) and using the effective hydrogen-like principle quantum number n^*. The use of effective quantum number increases the cross-sections at the ionization edge for low-lying levels and reduces them for some levels of high excitation that is more realistic than the original hydrogenic approximation. The quantum-mechanical cross-sections $\sigma_{\rm QM}(\nu)$ for the state $z\,^7\mathrm{P}^\circ$ are compared with the hydrogenic approximation $\sigma_{\rm hyd}(\nu)$ in Fig. 2. The cross-section at the photoionization edge, as well as the background, are larger than $\sigma_{\rm hyd}(\nu)$. There are also strong resonances at energies, where the solar atmospheric UV flux is sufficiently strong to produce the overionization of the $z\,^7\mathrm{P}^\circ$ state. Quantum-mechanical cross-sections for the other levels with excitation energies $E_{\rm exc} \approx 3 - 4$ eV show a similar behaviour. We will show in Sect. 3 that these levels dominate ionization balance in Cr I.

At present, there are no experimental and accurate theoretical data for ionization and excitation in Cr I by electron impact, as well as by inelastic collisions with H I. Thus, we rely on the commonly-used approximations. Cross-sections for continuum and allowed discrete transitions due to inelastic collisions with H I were computed with the formulae of Drawin (1969). This original recipe was developed for collisions between equal hydrogen-like particles, hence we apply a scaling factor $0 \leq S_{\rm H} \leq 5$ to the Drawin cross-sections. The final choice of $S_{\rm H}$ is discussed in Sect. 5.2. The rates of allowed and forbidden transitions due collisions with electrons are calculated from the formulae of van Regemorter (1962) and Allen (1973), respectively. The accuracy of the electron-impact cross-sections adopted in this work is not better than that for collisions with neutral atoms (Mashonkina 1996). However, the excitation and ionization balance in Cr I/Cr II, as well as abundances of Cr determined from the lines of both ionization stages, depend only weakly on the exact treatment of inelastic e^- collisions. Our calculations show that even in the solar atmosphere ionization rates due to collisions with H I atoms dominate over the rates of ionization by electrons for the majority of the Cr levels, exceeding the latter by nearly three orders of magnitude for the uppermost levels. Moreover, collisional ionization rates dominate over collisional excitation rates. In the atmospheres of metal-poor stars, where the number density of free electrons is smaller than in the Sun, collisional excitation in Cr I is fully controlled by neutral hydrogen.

In addition to the reference atomic model of Cr, which is described above, we construct several test models. These models are used to show how the statistical equilibrium of Cr changes under variation of different atomic parameters, like size of the model atom, cross-sections for collisional and radiative transitions.

2.2. Model atmospheres and spectrum synthesis

To maintain consistency in the abundance calculations, we have decided to use the same type of model atmospheres, as employed for the derivation of stellar parameters (see Sect. 5), microturbulence velocities, and metallicites of the objects investigated in this work. These are classical static 1D plane-parallel models MAFAGS-ODF without chromospheres (Fuhrmann et al. 1997). Line blanketing is treated with opacity distribution functions from Kurucz (1992). Convection is taken into account with the mixing-length theory (Böhm-Vitense 1958) and the mixing length is set to 0.5 pressure scale heights. This value was chosen by Fuhrmann et al. (1993) to provide simultaneously the best fitting of Balmer line profiles in the solar flux spectrum with $T_{\rm eff} = 5780$ K. Barklem et al. (2002) also suggest that the best fit of Balmer line profiles can be achieved with $\alpha = 0.5$. Stratifications of temperature and pressure in MAFAGS-ODF are similar to those given by other comparable models (see Fig. 15 in Grupp 2004).

The abundances of Cr were computed by a method of spectrum synthesis with the code SIU, kindly provided by T. Gehren (private communication). Standard line broadening mechanisms, including radiation and quadratic Stark damping, were taken into account. The line half-widths due to elastic collisions with H I are calculated using the cross-sections and velocity exponents tabulated by Anstee & O'Mara (1995). In Table 2, they are given in terms of van der Waals damping constants $\log C_6$, calculated for the temperature 6000 K.

3. Statistical equilibrium of Cr

The departures of atomic level populations $n_i^{\rm NLTE}$ from their LTE values $n_i^{\rm LTE}$ are best understood from the inspection of departure coefficients, defined as $b_i = n_i^{\rm NLTE}/n_i^{\rm LTE}$. The departure coefficients for selected Cr I and Cr II levels calculated for the solar model atmosphere ($T_{\rm eff} = 5780$ K, $\log g = 4.44$, [Fe/H] = 0, $\xi_{\rm t} = 0.9$ km s^{-1}) with different atomic models are shown as a function of continuum optical depth $\log \tau_{\rm c}$ at 500 nm in Fig. 3. We will mainly discuss NLTE effects in Cr I, because the majority of Cr II levels remain very close to LTE for the range of

[2] http://physics.nist.gov/PhysRefData/

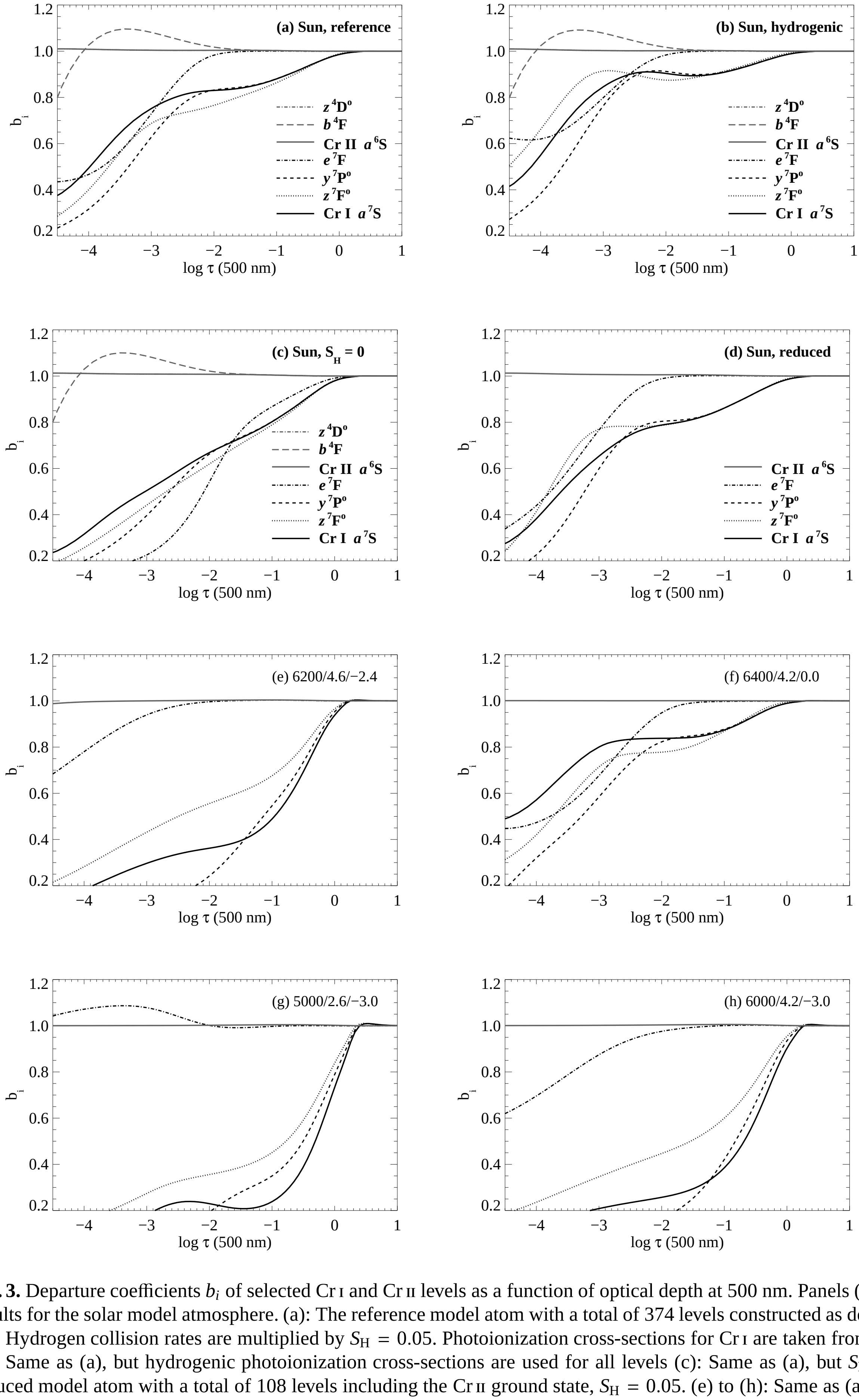

Fig. 3. Departure coefficients b_i of selected Cr I and Cr II levels as a function of optical depth at 500 nm. Panels (a) to (d) present results for the solar model atmosphere. (a): The reference model atom with a total of 374 levels constructed as described in Sect. 2.1. Hydrogen collision rates are multiplied by $S_{\rm H} = 0.05$. Photoionization cross-sections for Cr I are taken from Nahar (2009). (b): Same as (a), but hydrogenic photoionization cross-sections are used for all levels (c): Same as (a), but $S_{\rm H} = 0$. (d): The reduced model atom with a total of 108 levels including the Cr II ground state, $S_{\rm H} = 0.05$. (e) to (h): Same as (a), but the model atmospheres are taken from the grid with stellar parameters specified in each panel. Note that some levels on the plots are in thermal equilibrium with the other levels.

Table 1. Selected levels of Cr I in the model atom. Photoionization cross-sections at the edge $\sigma_{\rm thr}$ are adopted from Nahar (2009).

Level	g	$E_{\rm exc}$ eV	$\lambda_{\rm thr}$ Å	$\sigma_{\rm thr}$ Mb[a]	Level	g	$E_{\rm exc}$ eV	$\lambda_{\rm thr}$ Å	$\sigma_{\rm thr}$ Mb
$a\,^7$S	7	0.00	1832	0.099	$z\,^5$S°	5	5.35	8733	0.316
$a\,^5$S	5	0.94	2128	0.316	$e\,^5$D	25	5.46	9517	3.504
$a\,^5$D	25	1.00	2151	0.327	$w\,^5$P°	15	5.48	9645	4.793
$a\,^5$G	45	2.54	2936	0.001	$v\,^5$P°	15	5.57	10383	5.26
$a\,^5$P	15	2.71	3055	2.133	$f\,^7$S	7	5.66	11195	1.523
$z\,^7$P°	21	2.90	3209	25.02	$f\,^5$S	5	5.7	11617	2.613
$z\,^7$F°	49	3.15	3431	0.911	$f\,^7$D	35	5.8	12768	0.798
$z\,^5$P°	15	3.32	3599	27.3	$u\,^5$P°	15	5.82	13091	29.07
$z\,^7$D°	35	3.42	3708	6.884	$v\,^5$F°	35	5.91	14415	20.47
$y\,^7$P°	21	3.45	3741	0.89	$g\,^7$D	35	5.92	14554	19.71
$y\,^5$P°	15	3.68	4014	3.756	$w\,^7$P°	21	5.92	14565	38.33
$z\,^5$F°	35	3.85	4254	0.255	$u\,^5$F	35	5.95	15143	0.028
$a\,^5$F	35	3.89	4310	0.547	$f\,^5$D	25	6.04	16944	4.298
$z\,^5$D°	25	4.17	4779	0.545	$g\,^7$S	7	6.1	18526	2.968
$c\,^5$D	25	4.40	5241	19.14	$g\,^5$S	5	6.12	19033	4.949
$e\,^7$S	7	4.57	5656	0.537	$t\,^5$P°	10	6.17	20702	10.83
$e\,^5$S	5	4.7	5990	0.903	$s\,^5$F°	35	6.22	22667	40.11
$x\,^5$P°	15	5.08	7366	16.38	$u\,^5$D°	25	6.28	25238	3.526
$y\,^5$F°	35	5.11	7468	0.091	$h\,^5$S	5	6.33	28247	7.905
$y\,^5$D°	25	5.15	7687	1.267	$t\,^5$D	25	6.45	39357	4.353
$z\,^5$H°	55	5.23	8088	0.009	$r\,^5$F	35	6.58	68020	0.129
$e\,^7$D	35	5.24	8118	6.231	$h\,^7$D	32	6.62	86092	118.3
$x\,^7$P°	21	5.24	8119	27.37	$e\,^7$G	63	6.62	86731	151.0
$x\,^5$D°	25	5.29	8378	19.26					

[a] 1 Mb = 10^{-18}cm^2

stellar parameters we are interested in. As seen in the Grotrian diagram (Fig. 1), Cr is a very complex atomic system because a partially filled 3d electron shell results in a highly complex term structure with many low-lying and closely-spaced energy levels. Hence, in contrast to simpler atoms like Li (Shi et al. 2007, Fig. 2) or Na (Baumueller et al. 1998, Fig. 2), clear isolation of transitions driving departures from LTE is not trivial. We restrict the discussion of statistical equilibrium (SE) in Cr to few simple cases, which will be illustrated with a few levels characteristic for their depth dependency (Fig. 3).

The NLTE effects in Cr I are similar to that of the other minority atoms with complex configuration structure in cool stellar atmospheres, like Fe I, Mn I, and Co I. Deviations from LTE in Cr I develop in the layers where the mean intensity J_ν exceeds the Planck function $B_\nu(T_{\rm e})$ over the bound-free edges of significantly-populated low-lying Cr I levels. Analysis of radiative rates shows that the overionization is particularly strong from the odd levels with large photoionization cross-sections, e.g. $z\,^7$P° ($\lambda_{\rm thr}$ = 3209 Å, Fig. 2), $z\,^7$F° ($\lambda_{\rm thr}$ = 3431 Å), and $z\,^5$P° ($\lambda_{\rm thr}$ = 3599 Å). Thus, their b_i drop below unity already at $\log\tau_{\rm c} \sim +0.3$ (Fig. 3a). Overionization affects other low-excitation levels with $E_{\rm exc} \sim 2-4$ eV, although the net ionization rates are by orders of magnitude smaller then the rates from, e.g. $z\,^7$P° level. The cross-section of the ground state $a\,^7$S shows a number of autoionization resonances at $\lambda \leq 1700$ Å, where solar fluxes are too low to produce significant ionization. The Cr I ground state is underpopulated via resonance transition in the multiplet 4 ($a\,^7$S - $y\,^7$P°), which is in detailed balance at $\log\tau_{\rm c} \geq -1.5$, and via collisions with the lowest metastable states, which are overionized. A regular behaviour of departure coefficients for the majority of Cr I levels at $\log\tau_{\rm c} \geq -2$ confirms the dominance of radiative overionization at these depths with some deviations from relative thermal equilibrium between low levels (compare levels $z\,^7$F° and $a\,^7$S in Fig. 3a) reflecting the non-hydrogenic character of their photoionization cross-sections. We have also performed SE calculations with photoionization cross-sections for all Cr I levels derived from hydrogenic approximation. In this case, departure coefficients are homogeneously distributed up to the depths $\log\tau_{\rm c} \sim -1.5$ (Fig. 3b); b_i is a nearly monotonic function of the level ionization potential.

Line transitions influence Cr I excitation balance in the outer layers, $\log\tau_{\rm c} \leq -2$, where departure coefficients of the levels markedly deviate from unity and from each other (Fig. 3a). Pumping by superthermal radiation with $J_\nu > B_\nu(T_{\rm e})$ becomes important in the layers, where optical depth in the wings of strong low-excitation lines drops below unity. Detailed balance in the transitions does not hold and their upper levels are overpopulated. As soon as line cores form, $\tau_0^{\rm l} < 1$, spontaneous transitions depopulate the upper levels and their b_i steeply decrease. The spectrum of Cr I is represented by a large number of lines in the near-UV, which are subject to these non-equilibrium excitation effects. The transitions in the multiplet 4, which sustain thermal equilibrium between $a\,^7$S and $y\,^7$P° at $\log\tau_{\rm c} \geq -1$, now go out of the detailed balance and there is a small net radiative absorption leading to the overpopulation of $y\,^7$P° (Fig. 3a). At $\log\tau_{\rm c} \sim -3$, photon pumping ceases, because in the cores of the resonance lines $\tau_0^{\rm l} < 1$, hence the departure coeficient of the $y\,^7$P° level drops. The levels with $E_{\rm exc} \sim 2.9-3.4$ eV are radiatively connected with the uppermost levels, which are separated by an energy gap ≤ 0.5 eV from the continuum, e.g. transitions $y\,^7$P° - $e\,^7$F with $\lambda \sim 3880$ Å. Net radiative rates in these transitions are positive at $\log\tau_{\rm c} > -2$, but overpopulation of the upper levels does not occur because they are strongly coupled to the fully thermalized Cr II ground state. This coupling is maintained by collisions with H I, which exceed the respective rates of ionization due to collisions with electrons by few orders of magnitude. There is also a sequence of spontaneous de-excitations through the densely packed upper levels with $E_{\rm exc} \sim 5-6$ eV, which is driven by $J_\nu < B_\nu(T_{\rm e})$ at the corresponding frequencies.

Fig. 3c demonstrates the behaviour of Cr I level populations, when inelastic collisions with H I are neglected, $S_{\rm H} = 0$. Underpopulation of the levels at all optical depths is amplified, also the uppermost levels, like $e\,^7$F, decouple from the continuum already at $\log\tau_{\rm c} \approx 0$. Large differences with the reference model (Fig. 3a), computed with $S_{\rm H} = 0.05$, are seen at $\log\tau_{\rm c} < -1.5$, where electronic collisions are also not effective. Hence, we expect significant changes in the opacity of the cores of strong Cr I lines under NLTE. Also at $\log\tau_{\rm c} > -2$, departure coefficients of high-excitation levels are different from the case of $S_{\rm H} = 0.05$, thus affecting the source functions of intermediate-strength lines.

Similarly, removal of the high-excitation Cr I levels leads to slightly increased deviations from LTE in Cr I, although the variation of departure coefficients with depth at $-2 < \log \tau_c < 0$ is not different from the reference complete atomic model. Results for the reduced model atom, constructed with 108 levels of Cr I with excitation energy of the highest level 6.76 eV and closed by the Cr II state, are shown in Fig. 3d. This model is devoid of some doubly-excited Cr II states below the 1-st ionization threshold and only transitions with $\log gf > -1$ are included. Note the amplified underpopulation of the low and intermediate-excitation levels compared to the reference model. This result can be easily understood as due to the reduced radiative and collisional interaction of the Cr I levels with each other and with the continuum. Less electrons recombine and de-excite to the lower levels via weak infrared lines, where $J_\nu < B_\nu(T_e)$.

Statistical equilibrium of Cr in the atmospheres of cool subdwarfs and subgiants is established by radiative processes. NLTE effects on the levels of Cr I and Cr II are amplified compared to the solar case. The main reason is low abundances of metals, which supply free electrons and produce line blanketing in the short-wave part of a spectrum. Hence, increased UV fluxes at bound-free edges of low-excitation Cr I levels lead to their strong underpopulation, and collisional coupling between the levels is very weak due to deficient electrons. As an example, we consider a metal-poor turnoff star with [Fe/H] = −2.4 (Fig. 3e). Ionization balance is dominated by radiative transitions from the low-excitation Cr I levels. At $-1 < \log \tau_c < 0.2$, these levels are depopulated by overionization and by optical pumping in strong resonance lines, connecting the levels of $a\,^7$S and $y\,^7$P° terms. At $\log \tau_c < -1$, photon pumping ceases because the lines become optically thin, and spontaneous de-excitations maintain relatively constant b_i of the $a\,^7$S state in the outer layers. An interesting result is the presence of small deviations from LTE for intermediate-excitation Cr II levels. As seen on the Fig. 3e, the odd level $z\,^4$D° with excitation energy 6.2 eV is slightly overpopulated by optical pumping at $-2 < \log \tau_c < 0$. But at smaller depths, photon losses in transitions of the multiplet $b\,^4$F - $z\,^4$D° result in a depopulation of the upper level. We use the lines of this multiplet in the abundance analysis.

Effective temperature and gravity do not affect distribution of atomic level populations at solar metallicity, but they become important with decreasing [Fe/H]. The results for the model with $T_{\rm eff}$ = 6400 K, $\log g$ = 4.2, and [Fe/H]= 0 (Fig. 3f) are almost indistinguishable from those obtained with the solar model atmosphere at optical depths $\log \tau_c > -3$. This is stipulated by increased collisional interaction among the Cr I levels with $E_{\rm exc} > 3$ eV. Although the model flux maximum is shifted to shorter wavelengths, ground state ionization is still not efficient because the edge cross-section of the $a\,^7$S state is very low. In the cool model atmospheres, deviations from LTE depend on the stellar gravity, and the effect is most pronounced at low metallicity. At [Fe/H] = −3, departures from LTE for Cr I levels are stronger in the model with $T_{\rm eff}$ = 5000 K and $\log g$ = 2.6 then in the model with $T_{\rm eff}$ = 6000 K and $\log g$ = 4.2 (Fig. 3g, h). This may account for a systematic difference between metal-poor giants and dwarfs found by Lai et al. (2008) and Bonifacio et al. (2009) (see discussion in Sect. 5.2).

The atomic model of Cr used in this work is not computationally tractable in full NLTE calculations with 3D model atmospheres (see e.g. Botnen & Carlsson 1999, for Ca), which require reduction of the model. Our analysis suggests that it is possible to construct a simpler model of Cr atom, which inherits the basic properties of the complete model and has similar performance under restriction of different stellar parameters. In particular, removal of high-excitation levels and numerous weak transitions in the Cr I atom, whose main effect is to provide stronger coupling of levels, can be compensated by increasing collisional interaction between them. The carefully chosen scaling factor to inelastic H I collisions makes up for the missing transitions: for Cr I, the reduced model with 108 levels and $S_{\rm H} = 0.15$ gives a similar description of the statistical equilibrium in Cr for solar-type stars to the complete reference model with 340 levels and $S_{\rm H} = 0.05$. However, there are two important concerns. First, the fact that the simple model atom performs well in 1D does not guarantee that accurate results are obtained with the same atomic model with 3D convective model atmospheres (Asplund 2005). Also, substituting the multitude of levels and transitions in Cr I by increased efficiency of collisions with H I (although both seem to produce the same effect on level populations) has certainly no physical justification. In fact, our result even suggests that large scaling factors to the Drawin's formula, as sometimes encountered in the literature, may stem from the missing atomic data in SE calculations.

4. Solar lines of Cr I and Cr II

All lines selected for the solar abundance analysis are given in Table 2. We used the MAFAGS-ODF model atmosphere (Sect. 2) with solar parameters. The profiles are broadened by the solar rotation $V_{\rm rot,\odot}$ = 1.8 km s^{-1} , microturbulence velocity ξ_t = 0.9 km s^{-1} , and by a radial-tangential macroturbulence velocity $V_{\rm mac} = 2.5\ldots4$ km s^{-1}. Radial and tangential components of $V_{\rm mac}$ are assumed to be equal, and velocity distribution for each component is Gaussian. $V_{\rm mac}$ is allowed to vary with the line strength and depth of formation. The comparison spectrum was taken from the Solar Flux Atlas of Kurucz et al. (1984).

Oscillator strengths for the Cr I lines are taken from two sources. Most of the data are from Sobeck et al. (2007), who determined branching ratios of transitions by Fourier transform spectroscopy. The accuracy of $\log gf$ values is within 5 – 10% for majority of transitions. In the absence of data from Sobeck et al., we used transition probabilities from Blackwell et al. (1986) measured with the absorption technique. Fuhr et al. (1988) ascribe 10% accuracy to these values. Oscillator strengths for the majority of Cr II lines are taken from Nilsson et al. (2006). Branching ratios were measured with Fourier transform spectrometer and combined with lifetimes from laser-induced fluorescence experiment. The uncertainty of absolute oscillator strengths is 12 − 16% for the transitions used in this work, except for the Cr II line at 4592 Å with an uncertainty of 37%. For the lines at 4555 and 4812 Å,

Table 2. Lines of Cr I and Cr II selected for solar and stellar abundance calculations. Wavelengths λ and excitation energies of the lower levels of the transitions E_{low} are taken from NIST database. The multiplet is specified in the 3-d column. Solar $\log(gf\varepsilon)$ values for the lines with an asterisk in the wavelength entry can not be reliably computed due to severe blending. These lines are not used in determination of the solar Cr abundance.

Id.[a]	λ [Å]	Mult.	E_{low} [eV]	Lower level	Upper level	$\log gf$	$\log C_6$	$\log(gf\varepsilon)$
Cr I								
bl	4254.35*	1	0.00	$a\,^7\mathrm{S}_3$	$z\,^7\mathrm{P}^\circ_4$	-0.090	-31.54	-
bl	4274.80*	1	0.00	$a\,^7\mathrm{S}_3$	$z\,^7\mathrm{P}^\circ_3$	-0.220	-31.55	-
bl	4289.72*	1	0.00	$a\,^7\mathrm{S}_3$	$z\,^7\mathrm{P}^\circ_2$	-0.370	-31.55	-
bl	4373.25	22	0.98	$a\,^5\mathrm{D}_2$	$z\,^5\mathrm{F}^\circ_1$	-2.300	-31.72	3.46
	4492.31	197	3.38	$b\,^3\mathrm{P}_2$	$y\,^3\mathrm{S}^\circ_1$	-0.390	-31.34	5.34
bl. w	4496.86	10	0.94	$a\,^5\mathrm{S}_2$	$y\,^5\mathrm{P}^\circ_3$	-1.140	-31.62	4.61
	4535.15	33	2.54	$a\,^5\mathrm{G}_3$	$z\,^5\mathrm{G}^\circ_4$	-1.020	-31.59	4.74
	4541.07	33	2.54	$a\,^5\mathrm{G}_4$	$z\,^5\mathrm{G}^\circ_3$	-1.150	-31.59	4.58
	4545.96	10	0.94	$a\,^5\mathrm{S}_2$	$y\,^5\mathrm{P}^\circ_2$	-1.370	-31.63	4.39
bl. w	4591.39	21	0.97	$a\,^5\mathrm{D}_1$	$y\,^5\mathrm{P}^\circ_2$	-1.740	-31.75	4.01
bl	4600.75	21	1.00	$a\,^5\mathrm{D}_3$	$y\,^5\mathrm{P}^\circ_3$	-1.250	-31.74	4.49
bl. w	4613.37	21	0.96	$a\,^5\mathrm{D}_0$	$y\,^5\mathrm{P}^\circ_1$	-1.650	-31.76	4.13
	4616.14	21	0.98	$a\,^5\mathrm{D}_2$	$y\,^5\mathrm{P}^\circ_2$	-1.190	-31.75	4.54
	4626.19	21	0.97	$a\,^5\mathrm{D}_1$	$y\,^5\mathrm{P}^\circ_1$	-1.330	-31.76	4.42
	4633.29	186	3.13	$z\,^7\mathrm{F}^\circ_3$	$f\,^7\mathrm{D}_4$	-1.110	-31.18	4.62
	4646.17	21	1.03	$a\,^5\mathrm{D}_4$	$y\,^5\mathrm{P}^\circ_3$	-0.740	-31.74	5.01
bl. w	4651.28	21	0.98	$a\,^5\mathrm{D}_2$	$y\,^5\mathrm{P}^\circ_1$	-1.460	-31.75	4.30
bl. w	4652.16	21	1.00	$a\,^5\mathrm{D}_3$	$y\,^5\mathrm{P}^\circ_2$	-1.040	-31.75	4.71
	4700.61	62	2.71	$a\,^5\mathrm{P}_1$	$z\,^5\mathrm{S}^\circ_2$	-1.255	-31.61	4.51
bl	4708.04	186	3.17	$z\,^7\mathrm{F}^\circ_5$	$f\,^7\mathrm{D}_4$	0.07	-31.18	5.83
bl. w	4745.31	61	2.71	$a\,^5\mathrm{P}_3$	$x\,^5\mathrm{D}^\circ_4$	-1.380	-31.17	4.33
	4801.03	168	3.12	$a\,^3\mathrm{F}_4$	$y\,^3\mathrm{F}^\circ_3$	-0.131	-31.35	5.62
bl	4885.78*	30	2.54	$a\,^5\mathrm{G}_3$	$x\,^5\mathrm{P}^\circ_2$	-1.055	-31.3	-
	4936.33	166	3.11	$a\,^3\mathrm{F}_3$	$z\,^3\mathrm{H}^\circ_4$	-0.25	-31.37	5.47
	4953.72	166	3.12	$a\,^3\mathrm{F}_4$	$z\,^3\mathrm{H}^\circ_4$	-1.48	-31.37	4.23
bl	5204.52*	7	0.94	$a\,^5\mathrm{S}_2$	$z\,^5\mathrm{P}^\circ_1$	-0.19	-31.36	-
bl	5206.04	7	0.94	$a\,^5\mathrm{S}_2$	$z\,^5\mathrm{P}^\circ_2$	0.02	-31.36	5.67
bl	5208.44	7	0.94	$a\,^5\mathrm{S}_2$	$z\,^5\mathrm{P}^\circ_3$	0.17	-31.36	5.83
	5241.46	59	2.71	$a\,^5\mathrm{P}_1$	$x\,^5\mathrm{P}^\circ_1$	-1.920	-31.3	3.74
bl. w	5243.40	201	3.40	$z\,^7\mathrm{D}^\circ_2$	$f\,^7\mathrm{D}_1$	-0.580	-31.22	5.17
	5247.56	18	0.96	$a\,^5\mathrm{D}_0$	$z\,^5\mathrm{P}^\circ_1$	-1.590	-31.41	4.28
	5272.01	225	3.45	$y\,^7\mathrm{P}^\circ_3$	$f\,^7\mathrm{D}_4$	-0.420	-31.2	5.31
	5287.19	225	3.44	$y\,^7\mathrm{P}^\circ_2$	$f\,^7\mathrm{D}_3$	-0.870	-31.21	4.84
	5296.69	18	0.98	$a\,^5\mathrm{D}_2$	$z\,^5\mathrm{P}^\circ_1$	-1.360	-31.41	4.49
	5300.75	18	0.98	$a\,^5\mathrm{D}_2$	$z\,^5\mathrm{P}^\circ_3$	-2.000	-31.41	3.73
bl. w	5304.21	225	3.46	$y\,^7\mathrm{P}^\circ_4$	$f\,^7\mathrm{D}_4$	-0.670	-31.2	5.04
	5312.88	225	3.45	$y\,^7\mathrm{P}^\circ_3$	$f\,^7\mathrm{D}_3$	-0.550	-31.21	5.17
	5318.78	225	3.44	$y\,^7\mathrm{P}^\circ_2$	$f\,^7\mathrm{D}_2$	-0.670	-31.22	5.04
	5340.44	225	3.44	$y\,^7\mathrm{P}^\circ_2$	$f\,^7\mathrm{D}_1$	-0.730	-31.22	5.02
	5345.81	18	1.00	$a\,^5\mathrm{D}_3$	$z\,^5\mathrm{P}^\circ_2$	-0.95	-31.41	4.87
	5348.32	18	1.00	$a\,^5\mathrm{D}_3$	$z\,^5\mathrm{P}^\circ_3$	-1.21	-31.41	4.60
bl. w	5409.79	18	1.03	$a\,^5\mathrm{D}_4$	$z\,^5\mathrm{P}^\circ_3$	-0.670	-31.41	5.15
	5628.64	203	3.42	$b\,^3\mathrm{G}_3$	$z\,^3\mathrm{H}^\circ_4$	-0.740	-31.34	4.99
Cr II								
	4555.00	44	4.07	$b\,^4\mathrm{F}_3$	$z\,^4\mathrm{D}^\circ_3$	-1.25	-32.4	4.42
	4558.66	44	4.07	$b\,^4\mathrm{F}_4$	$z\,^4\mathrm{D}^\circ_3$	-0.66	-32.4	5.30
bl	4588.22	44	4.07	$b\,^4\mathrm{F}_3$	$z\,^4\mathrm{D}^\circ_2$	-0.83	-32.4	5.08
	4592.09	44	4.07	$b\,^4\mathrm{F}_2$	$z\,^4\mathrm{D}^\circ_2$	-1.42	-32.4	4.47
bl	4634.11	44	4.07	$b\,^4\mathrm{F}_1$	$z\,^4\mathrm{D}^\circ_0$	-0.98	-32.4	4.69
bl	4812.35	30	3.86	$a\,^4\mathrm{F}_3$	$z\,^4\mathrm{F}^\circ_4$	-2.10	-32.46	3.73
bl	4824.14	30	3.87	$a\,^4\mathrm{F}_4$	$z\,^4\mathrm{F}^\circ_4$	-0.92	-32.46	5.01
bl	5237.34	43	4.07	$b\,^4\mathrm{F}_4$	$z\,^4\mathrm{F}^\circ_4$	-1.16	-32.4	4.51
bl	5308.44	43	4.07	$b\,^4\mathrm{F}_3$	$z\,^4\mathrm{F}^\circ_2$	-1.81	-32.4	3.84
	5313.59	43	4.07	$b\,^4\mathrm{F}$	$z\,^4\mathrm{F}^\circ$	-1.65	-32.4	4.09

we used the $\log gf$'s from Wujec & Weniger (1981), and the Cr II lines of multiplet 43 were calculated with $\log gf$'s derived from the solar spectrum analysis by Kostyk & Orlova (1983). The accuracy of $\log gf$ values from Wujec & Weniger (1981) and Kostyk & Orlova (1983) was later revised by Fuhr et al. (1988) to be of the order of 50%.

The LTE abundance of Cr determined from the Cr I lines is $\log\varepsilon = 5.66 \pm 0.04$ dex, where the uncertainty is one standard deviation. Our LTE abundance is consistent with the meteoritic value, 5.63 ± 0.01 dex[3]. Sobeck et al. (2007) calculated $\log\varepsilon = 5.64 \pm 0.04$ dex from equivalent widths of Cr I lines in the disk-center intensity spectrum. The agreement of our LTE abundance and that of Sobeck et al. is surprising, since these authors used a semi-empirical Holweger-Müller model atmosphere and assumed a lower value of the microturbulence velocity, $\xi_t = 0.8$ km s^{-1}. The abundances of Cr based on the LTE analysis of Cr II lines are similar in our study and in Sobeck et al., 5.81 ± 0.13 dex and 5.77 dex with $\sigma = 0.13$ dex, respectively.

The LTE analysis of Cr lines revealed two problems. First, there is an abundance discrepancy of ~ 0.15 dex between Cr I and Cr II lines, which also appears in the study of Sobeck et al. The line-to-line abundance scatter for Cr II is also large, $\sigma = 0.13$ dex. Second, there is a large spread of abundances within the multiplet 18: profile fitting of the Cr I lines with equivalent widths $W_\lambda > 60$ mÅ requires systematically higher abundances by ~ 0.1 dex compared to weaker lines. A similar discrepancy was noted by Blackwell et al. (1987), who explained this with non-thermal excitation in the multiplet 18. Sobeck et al. did not support the Blackwell's conclusion, although a 0.1 dex line-to-line scatter in this multiplet is also present in their results. We show in the next paragraph, whether either of these two problems can be solved with NLTE.

The NLTE line formation is based on the departure coefficients b_i computed with the reference model of Cr atom (Sect. 2). We performed test calculations for two scaling factors to inelastic collisions with hydrogen, $S_{\mathrm{H}} = 0$ and 0.05. In both cases, NLTE corrections to abundances derived from Cr I lines are positive and range from 0.05 to 0.1 dex, depending on the line strength and the excitation potential of the lower level. All Cr I lines computed under NLTE with $S_{\mathrm{H}} = 0$ fit the observed spectrum with the Cr abundance $\log\varepsilon = 5.74 \pm 0.05$ dex, whereas a scaling factor $S_{\mathrm{H}} = 0.05$ leads to $\log\varepsilon = 5.7 \pm 0.04$ dex. The NLTE abundance corrections to the Cr II lines are small and negative. The results for $S_{\mathrm{H}} = 0$ and $S_{\mathrm{H}} = 0.05$ are equal, $\log\varepsilon = 5.79 \pm 0.12$ dex. In contrast to LTE, the difference between both ionization stages is now fairly small, $\log\varepsilon(\mathrm{Cr\,II}) - \log\varepsilon(\mathrm{Cr\,I}) = 0.05$ dex for $S_{\mathrm{H}} = 0$, and it is within the combined errors of both values. At present, we can not determine what causes the discrepancy between the abundance of Cr in meteorites and our NLTE 1D abundance for the solar photosphere. The accuracy claimed for oscillator strengths of Cr II and Cr I transitions measured by Nilsson et al. (2006) and Sobeck et al. (2007), respectively, is very high. There is evi-

[3] The Cr abundance in CI-chondrites from Lodders et al. (2009) was renormalized to the photospheric Si abundance of Shi et al. (2008), $\log\varepsilon_{\mathrm{Si},\odot} = 7.52$ dex

dence that lines of a similar atom Fe I are affected by convective surface inhomogeneities, also NLTE effects on Fe I lines are different in 1D and in 3D radiative transfer calculations (see below). For Cr, such detailed investigations are not yet available.

Our reference NLTE model satisfies ionization equilibrium of Cr, but it does not solve the problem of overestimated abundances from several lines of multiplet 18. The solar NLTE abundance corrections[4] $\Delta_{\rm NLTE}$ for all lines of this multiplet are equal and they scale with the $S_{\rm H}$ parameter. The behaviour of line profiles under NLTE can be understood from the analysis of level departure coefficients b_i at the depths of line formation. The formation of weak lines with $W_\lambda < 60$ mÅ is confined to $-1 < \log\tau_{\rm c} < 0$, where $b_i = b_j$, so line source functions are thermal, $S_{\rm ij} = B_\nu$. Hence, line intensity profiles reflect the profile of an absorption coefficient, $\kappa_\nu \sim b_i$. Since $b_i < 1$, the lines are weaker relative to their LTE strengths and $\Delta_{\rm NLTE}$ is positive. Radiation in stronger lines of the multiplet 18 comes from the depths $-4 < \log\tau_{\rm c} < 0$. The line cores have lower intensities under NLTE due to depleted source functions, $S_{\rm ij} < B_\nu$, at $\log\tau_{\rm c} < -2$. But their wings, which dominate the total line strength, are formed at the depths where $b_i < 1$ due to overionization. The net effect on the line profile is that the NLTE abundance correction is positive. For all lines of multiplet 18, we find $\Delta_{\rm NLTE} \approx +0.1$ dex and +0.05 dex for $S_{\rm H} = 0$ and $S_{\rm H} = 0.05$, respectively. The result is incompatible with the suggestion of Blackwell et al. (1987), since the latter would require NLTE effects of different magnitude for all lines of multiplet 18. Moreover, in our 'extreme' NLTE model with $S_{\rm H} = 0$, the net NLTE effect on the profiles of stronger lines must be zero to eliminate the abundance scatter. If this problem is due to a deficiency of the atomic model, our main concern is the crude approximation used for inelastic collisions with H I. Compared to the Drawin's formulae, *ab initio* quantum-mechanical calculations (Belyaev et al. 1999; Belyaev & Barklem 2003) predict significantly lower collision rates for certain transitions of simple alkali atoms, and they show that, in addition to excitation, other effects like ion-pair formation become important. Thus, in principle, any rescaling of the Drawin's cross-sections, e.g. using variable $S_{\rm H}$ for levels of different excitation energies as exemplified by Baumueller & Gehren (1996), does not improve the reliability of results. Variation of $S_{\rm H}$ does not reduce the scatter among the Cr II lines, because the NLTE effects are very small even for $S_{\rm H} = 0$. For the same reason, employment of an LTE versus a NLTE approach does not decrease the scatter.

The abundance anomaly among some Cr I and Cr II lines may reflect shortcomings of the 1D static mixing-length model atmospheres. Discrepant Cr I and Cr II lines with $70 < W_\lambda < 120$ mÅ are very sensitive to a variation of the microturbulence parameter that was also demonstrated for Fe I lines with similar equivalent widths (Gehren et al. 2001b). For $\Delta\xi_{\rm t} = \pm 0.2$ km s^{-1} with respect to the reference value 0.9 km s^{-1}, the abundances derived from the Cr I lines of multiplet 18 change by roughly ∓0.1 dex, and any combination of $\xi_{\rm t}$ and $\log\varepsilon$ leads to an equally good profile fit (Fig. 4). Using the depth-dependent microturbulence as suggested by Holweger (1967) does not eliminate the abundance scatter among Cr I lines, although the Cr II lines are strengthened requiring 0.1 – 0.15 dex lower abundances.

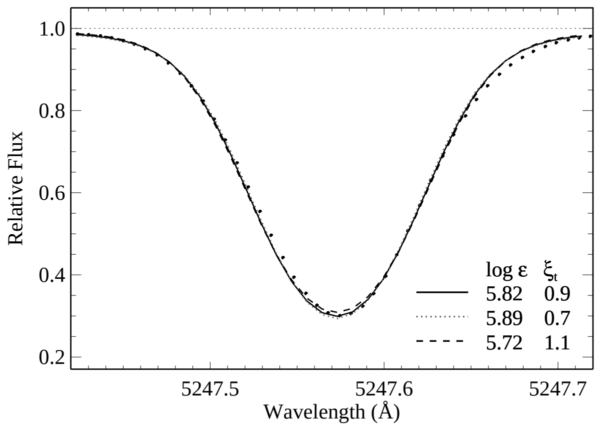

Fig. 4. NLTE profiles of the Cr I line at 5247 Å. Different combinations of microturbulent velocities $\xi_{\rm t}$ and resulting Cr abundances $\log\varepsilon$ are shown. The line shows a convective asymmetry.

Clearly, our approach of solving line formation in 1D homogeneous models with a two-component gaussian velocity field is simple compared to multidimensional radiative transfer calculations (e.g. Asplund et al. 2000). Steffen & Holweger (2002) have shown that abundance corrections due to photospheric temperature fluctuations vary in sign and magnitude for lines of different $E_{\rm low}$, λ, and W_λ. For saturated lines, some effect due to hydrodynamic velocity fields are also predicted. Besides, there is evidence that NLTE effects on atomic level populations are amplified in the presence of convective surface inhomogeneities (e.g. Shchukina & Trujillo Bueno 2001, for the Sun). Neutral iron is strongly overionized above hot granules compared to cooler intergranular regions with the maximum effect on the opacity of low-excitation Fe I lines with $E_{\rm low} < 2$ eV. Deviations of the source function from $B_\nu(T_{\rm e})$ are important for higher-excitation lines in the intergranular regions. Shchukina & Trujillo Bueno also find that strong lines of any excitation potential formed above $\log\tau_{\rm c} \sim -2.5$ are sensitive to the variation of collision rates. Comparable effects can be expected for the lines of Cr I, hence a systematic study of 3D effects in Cr is necessary to confirm this. Asplund et al. (2009) computed LTE line formation for Cr I and Cr II with a hydrodynamical model atmosphere. Applying NLTE abundance corrections derived from our 1D modelling, Asplund et al. obtained the solar Cr abundance 5.64 ± 0.04 dex, which is almost equal to our LTE 1D solar abundance determined from the Cr I lines. Another study, which provides an order-of-magnitude estimate of 3D effects on the Cr line formation in very metal-poor atmospheres, is Bonifacio et al. (2009). We briefly discuss this paper in Sect. 5.2.

[4] The difference in abundances required to fit LTE and NLTE profiles is referred to as the NLTE abundance correction, $\Delta_{\rm NLTE} = \log\varepsilon^{\rm NLTE} - \log\varepsilon^{\rm LTE}$

Finally, we note that all problematic Cr II lines are located in the spectral region 4500 – 4800 Å, where the continuum level is uncertain due to severe blending. Hence, the abundance discrepancy may be, at least in part, removed by adjusting the local continuum. On the other side, this procedure could also affect Cr I lines located in this spectral region.

5. Abundances of Cr in metal-poor stars

5.1. Observations and stellar parameters

The list of stars along with their parameters is given in Table 3. Most of the stars were observed by T. Gehren and collaborators with UVES spectrograph at the VLT UT2 on the Paranal, Chile, in 2001, and/or with the FOCES echelle spectrograph mounted at the 2.2m telescope of the CAHA observatory on Calar Alto. The observations of HD 84937 were taken from the UVESPOP survey (Bagnulo et al. 2003). The UVES spectrum for G 64-12 was taken from ESO/ST-ECF Science Archive Facility (PID 67.D-0554(A)). With the spectral resolution of $\lambda/\Delta\lambda \sim 40\,000 - 60\,000$, it is not possible to distinguish the contribution of $V_{\rm mac}$ and $V_{\rm rot}$ to a line profile. Hence, the profiles are convolved with a Gaussian with the full width at half maximum $\sim 2.8 - 4$ km s^{-1}.

The sample includes nine objects from our recent studies (Bergemann & Gehren 2008; Bergemann et al. 2009), where the details on observational material and derivation of stellar parameters can be found. In addition, we include here one thin disk star, HD 123710. Parameters of all these stars are determined by Gehren et al. (2004, 2006) using the same MAFAGS-ODF model atmospheres, as employed in this work. The effective temperatures were obtained from fitting the Balmer line profiles under LTE. The spectroscopic temperatures are in agreement with the $T_{\rm eff}$'s determined by the method of Infrared Fluxes (Alonso et al. 1996, 1999; Casagrande et al. 2010). The offset with $T_{\rm eff}$'s from the last reference is $\sim$ 20 K with an *rms* error 23 K. Surface gravities are based on *Hipparcos* parallaxes.

Metallicities and microturbulence parameters were determined from LTE fitting of Fe II lines by requiring a zero slope of Fe abundances versus line equivalent widths. The validity of LTE approach in 1D line formation calculations for Fe II was demonstrated in very accurate analyses of statistical equilibrium of Fe in the Sun (Gehren et al. 2001a,b) and in metal-poor stars (Mashonkina et al. 2010). These studies employ the same type of atmospheric models, as we use in the current work.

Gehren et al. (2004, 2006) estimate the errors to be 100 K for $T_{\rm eff}$, 0.05 dex for $\log g$, 0.05 dex for [Fe/H], and 0.2 km/s for $\xi_{\rm t}$. For the halo and thick disk stars, the model atmospheres were computed with a total α-element enhancement of 0.4 dex.

5.2. [Cr/Fe] abundance ratios

The abundances of Cr in metal-poor stars are calculated strictly relative to the Sun. Any abundance estimate derived from a single line in a spectrum of a metal-poor star is referred to that from the corresponding solar line, which excludes the use of absolute oscillator strengths and of the average solar abundance. We derive a differential element abundance for each detected Cr line in a spectrum of a star according to

$$[{\rm El/H}] = \log(g f \varepsilon)^{*} - \log(g f \varepsilon)^{\odot}$$

and then we average over all these lines for a given ionization stage. Most of the Cr lines analyzed in the solar spectrum become very weak at low metallicities, so typically we use from 3 to 10 lines for each ionization stage.

Fig. 5 displays the difference between [Cr/Fe] ratios computed from the lines of two ionization stages, $[{\rm Cr_{II}/Cr_{I}}] = [{\rm Cr_{II}/Fe}]$ - $[{\rm Cr_{I}/Fe}]$, as a function of stellar effective temperature and metallicity. NLTE and LTE ratios are shown with filled and open symbols, respectively. NLTE abundances are based on SE calculations with the atomic model of Cr with $S_{\rm H} = 0$. There is an offset of $\sim$ 0.2 – 0.3 dex between Cr I and Cr II lines under LTE, which increases with decreasing [Fe/H] (Fig. 5, bottom). This reflects the fact that the main stellar parameter that controls deviations from LTE in Cr is the metal abundance. Since the NLTE effects of gravity and effective temperature are smaller than that of [Fe/H], we do not see a clear trend with $T_{\rm eff}$ in Fig. 5 (top), where no pre-selection according to $\log g$ or [Fe/H] was made. A discrepancy of a similar magnitude and sign was reported by Johnson (2002), Lai et al. (2008), and Bonifacio et al. (2009). All studies agree that for giants with $T_{\rm eff} \leq 5000$ the difference between two ionization stages is $\sim$ 0.4 dex. For hotter and higher-gravity models, characteristic of dwarfs, Lai et al. and Bonifacio et al. derive smaller offsets, $[{\rm Cr_{II}/Cr_{I}}] \sim 0.2$ dex, in good agreement with our LTE calculations. These findings are consistent with differential NLTE effects in Cr, which at low metallicity are larger for low $\log g$ and low $T_{\rm eff}$ models corresponding to giants (Sect. 3).

Our main result is that the offset between Cr I and Cr II for any combination of stellar parameters investigated here disappears when we use atomic level populations computed with the reference atomic model with $S_{\rm H} = 0$ (Fig. 5). This model allows for extreme NLTE effects on Cr I due to neglect of thermalizing H I collisions. For $S_{\rm H} = 0.05$, the abundances based on the Cr I lines decrease by ≤ 0.05 dex. Although these results are close to the abundances computed with $S_{\rm H} = 0$, the agreement between two ionization stages is not so good, $[{\rm Cr_{II}/Cr_{I}}] \sim 0.04 \ldots 0.07$ dex, and the offset becomes even larger with increasing $S_{\rm H}$.

The average Cr abundances for each star and their standard deviations are given in Table 3. Table 4 with individual abundances for each line of Cr I and Cr II is available in the electronic edition of A&A. $[{\rm Cr_{I}/Fe}]$ and $[{\rm Cr_{II}/Fe}]$ refer to the analysis of Cr I and Cr II lines, respectively. NLTE abundances given in this table were computed with $S_{\rm H} = 0$. In the spectra of BD$-4^{\circ}3208$ and G 64-12 no lines of Cr II were detected, and $[{\rm Cr_{II}/Fe}]$ value for HD 140283 is based on one Cr II line. In Fig. 6, [Cr/Fe] ratios computed under NLTE and LTE are plotted as a function of the stellar iron abundance, with [Fe/H] based on the LTE analysis of Fe II lines. The mean NLTE [Cr/Fe] ratio in stars with subsolar metallicity is $\langle[{\rm Cr/Fe}]\rangle = 0$ with the dispersion $\sigma = 0.06$ dex. Assuming LTE, we derive $\langle[{\rm Cr/Fe}]\rangle = -0.21$ with $\sigma = 0.11$ dex. The mean LTE value $\langle[{\rm Cr/Fe}]\rangle$ and the slope of [Cr/Fe] with [Fe/H] agree with other comparison studies, which refer

Table 3. Stellar parameters for the selected sample. NLTE and LTE abundances of Cr computed using the lines of Cr I and Cr II are given as $[\mathrm{Cr_I/Fe}]$ and $[\mathrm{Cr_{II}/Fe}]$, respectively. The standard deviations of these values are quoted as errors. The abundances of Fe are based on Fe II lines. $N_{\mathrm{Cr\,I}}$ and $N_{\mathrm{Cr\,II}}$ are the number of Cr I and Cr II lines used for each star. See text for further discussion of the data.

Object	T_{eff}	$\log g$	ξ_t	[Fe/H]	$N_{\mathrm{Cr\,I}}$	$N_{\mathrm{Cr\,II}}$	$[\mathrm{Cr_I/Fe}]$		$[\mathrm{Cr_{II}/Fe}]$		[Mg/Fe]
	K		km/s				NLTE	LTE	NLTE	LTE	
HD 19445	5985	4.39	1.5	−1.96	7	3	−0.07 ± 0.05	−0.3 ± 0.06	−0.09 ± 0.01	−0.11 ± 0.03	0.38
HD 34328	5955	4.47	1.3	−1.66	12	3	0.01 ± 0.04	−0.16 ± 0.03	0.02 ± 0.02	−0.01 ± 0.02	0.42
HD 84937	6346	4.00	1.8	−2.16	9	2	0.01 ± 0.05	−0.24 ± 0.06	−0.02 ± 0.02	−0.08 ± 0.04	0.32
HD 102200	6120	4.17	1.4	−1.28	16	4	0.01 ± 0.06	−0.11 ± 0.06	0.01 ± 0.03	0.0 ± 0.04	0.34
BD−4°3208	6310	3.98	1.5	−2.23	6	0	0.04 ± 0.03	−0.24 ± 0.03			0.34
HD 122196	5957	3.84	1.7	−1.78	10	2	−0.09 ± 0.05	−0.32 ± 0.06	−0.03 ± 0.02	−0.06 ± 0.04	0.24
HD 123710	5790	4.41	1.4	−0.54	14	4	−0.02 ± 0.03	−0.04 ± 0.03	−0.02 ± 0.03	−0.02 ± 0.02	0.24
HD 148816	5880	4.07	1.2	−0.78	21	6	0.01 ± 0.05	−0.06 ± 0.07	0.0 ± 0.05	0.0 ± 0.04	0.36
HD 140283	5773	3.66	1.5	−2.38	8	1	−0.03 ± 0.06	−0.38 ± 0.04	0.0	−0.08	0.43
G 64-12	6407	4.20	2.3	−3.12	4	0	0.13 ± 0.04	−0.26 ± 0.02			0.33

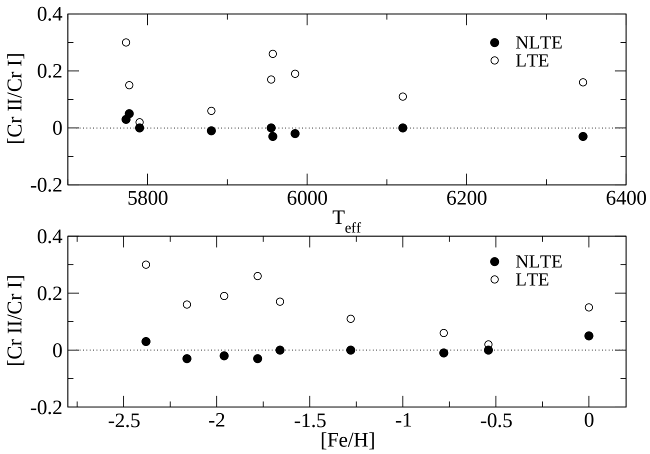

Fig. 5. [Cr/Fe] ratios as determined from Cr I and Cr II lines under NLTE (filled symbols) and LTE (open symbols) as a function of effective temperature (top) and metallicity (bottom) for selected stars. The NLTE abundances are computed with $S_{\mathrm{H}} = 0$.

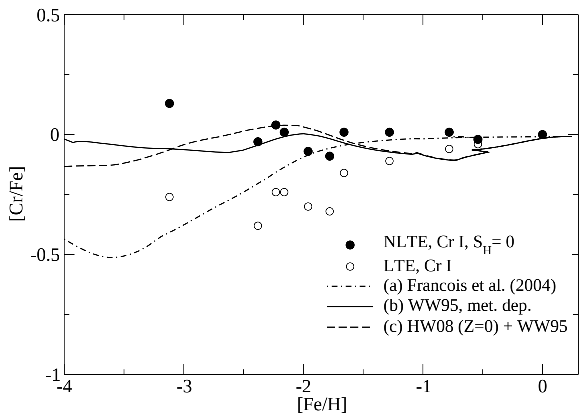

Fig. 6. Abundance ratios [Cr/Fe] as a function of metallicity. NLTE and LTE-based Cr abundances in metal-poor stars are marked with filled and open symbols. The evolutionary curves for [Cr/Fe] are computed with the CE model for the solar neighborhood adopting different sets of SN II yields (a) - (c).

to the LTE analysis of Cr I lines. Cayrel et al. (2004) showed that [Cr/Fe] ratios in giants increase from −0.5 at [Fe/H] ≈ −4 to −0.25 at [Fe/H] ≈ −2, and the scatter in abundance ratios is very small, σ = 0.05 dex. Such a small dispersion contradicts earlier results of McWilliam et al. (1995) and Ryan et al. (1996), who demonstrate a large spread of [Cr/Fe] abundances at any given metallicity. The reason for this disagreement is that Cayrel et al. (2004) investigated only giant stars, whereas the analysis of McWilliam et al. (1995) and Ryan et al. (1996) are based on a compilation of their own LTE measurements in a mixed sample of stars and on other data from the literature.

The mean LTE abundances in metal-poor stars based on the Cr II lines are identical in our study and in Gratton & Sneden (1991), ⟨[Cr/Fe]⟩ = −0.05 ± 0.04 dex and −0.04 ± 0.05 dex, respectively. Both of these values are consistent with the mean NLTE abundance derived from the Cr I lines. This is not surprising, because we find minor NLTE effects in Cr II for the range of stellar parameters investigated here and excellent agreement is achieved between the Cr I and Cr II lines under NLTE.

Recently, Bonifacio et al. (2009) performed an LTE analysis of Cr abundances in very metal-poor dwarfs and giants, demonstrating the influence of multidimensional RT effects on Cr I line formation in low-metallicity model atmospheres. For giants, they determine a factor of 2 smaller 3D-1D abundance corrections than for dwarfs. Although this result may explain the systematic offset of 0.2 dex, which they find between evolved and turnoff stars, it is not clear how these 3D effects will manifest themselves in full 3D NLTE RT calculations.

6. Chemical evolution model for [Cr/Fe] ratio

6.1. Nucleosynthesis

Calculations of stellar nucleosynthesis and Galactic chemical evolution indicate that the solar abundances of Fe and Cr derive for about 2/3 from SNe Ia and the residue from SNe II (Matteucci & Greggio 1986; Samland 1998). In both instances, the formation of these even-Z iron peak elements occurs in explosive burning of silicon (Hix & Thielemann 1999; Thielemann et al. 2007). ^{52}Cr, which constitutes 83.8% of the solar Cr abundance, is formed as radioactive ^{52}Fe mainly in the incomplete Si-burning region (Umeda & Nomoto 2002, 2005). The dominant isotope of Fe, ^{56}Fe (91.7% of the solar Fe abundance) is produced as radioactive ^{56}Ni at very high temperatures, $T > 4 \cdot 10^9 K$ (Woosley & Weaver 1995). Since both ^{52}Cr and ^{56}Fe are formed as α-particle nuclei, the total yields of Cr and Fe are almost independent of the neutron excess in the matter undergoing explosive burning and, to a first order, of the metallicity of SN progenitors.

Although the nucleosynthesis sites for Cr and Fe are identified, theoretical stellar yields of these elements are subject to large uncertainties related to modelling the SN explosion. The amount of Fe-peak elements ejected in a SN II primarily depends on the explosion energy and on the the mass cut between the ejected material and the collapsed core (note that these parameters are related, although they are often treated independently, e.g. Umeda & Nomoto (2002)). Less Cr is produced relative to Fe for deeper mass cut (Nakamura et al. 1999; Umeda & Nomoto 2002). The current crude estimates of the mass cut are based on the mass ejected in the form of ^{56}Ni and on the ratio ^{58}Ni/^{56}Ni, which are determined from SN II light curves and spectra. Other parameters, which affect the relative production of Fe-group nuclei, are the degree of mixing and fallback to the remnant, energy and geometry of explosion (Nakamura et al. 1999; Umeda & Nomoto 2002, 2005). Nagataki et al. (1997) demonstrated that an axisymmetric explosion in SN II models enhances the production of ^{52}Cr. All these parameters are interlinked and depend on preceding stages of stellar evolution determined by initial physical properties of a star.

The yields of Fe-peak elements from SNe Ia are also rather uncertain. It is not clear what type of binary system evolution leads to an explosion, i.e. double or single degenerate scenario, and whether the explosion proceeds via delayed detonation or fast deflagration mechanism (see Iwamoto et al. 1999, and references therein). The production of neutron-rich isotopes in carbon deflagration models depends on the neutron excess η, which in turn depend on the ignition density and flame propagation speed. For exampple, Iwamoto et al. (1999) found that the yield of a neutron-rich ^{54}Cr isotope in the widely-used W7 model is very sensitive to η in the central region of a white dwarf model, where it is determined by electron captures on nuclei. In this SN Ia model, the neutron-rich isotope of iron ^{58}Fe is produced in the outer regions where η stems from CNO-cycle production of ^{14}N, i.e. the abundance of ^{58}Fe is correlated with initial metallicity of a white dwarf. Thus, depending on SN Ia model parameters, different isotopic abundance ratios for Cr and Fe can be obtained. Some fine-tuning of a SN Ia model may be necessary to reproduce the solar isotopic composition.

6.2. Model of chemical evolution

The results we obtain for the chemical evolution of Cr for the solar neighborhood are based on the model of François et al. (2004), which is a revised version of the two-infall model presented by Chiappini et al. (1997). This model assumes two episodes for the Galaxy formation: the first forms the halo on a short timescale of $\sim$ 1 Gyr, the second, much longer with a timescale of $\sim$ 7 Gyr, produces the disc. The initial mass function is adopted from Scalo (1986) and the star formation law is the one proposed originally by Talbot & Arnett (1975). Further details on the model can be found in François et al. (2004).

The following prescriptions for Fe-peak nucleosynthesis are adopted. For SN Ia, we use the metallicity-independent yields of Cr and Fe computed by Iwamoto et al. (1999) with the updated version of Chandrasekhar mass W7 model of Nomoto et al. (1984). This model predicts that $\sim$ 9% of the total solar Cr is in the form of ^{54}Cr. Hence, we have decreased the yield of the neutron-rich isotope ^{54}Cr by a factor of 4 in order to reproduce the solar abundance ratio of Cr isotopes. The overproduction of ^{54}Cr can be avoided in other SN Ia models with lower central ignition density and neutron excess (Iwamoto et al. 1999). We use three sets of massive star yields. The first set (a) is metallicity-independent yields from Woosley & Weaver (1995) (WW95), computed with the SN II models with a solar composition. We increased the Cr yields by a factor of 10 for the $10 - 20 M_\odot$ models following the recommendation of François et al. (2004), who used this trick to avoid strong underproduction of Cr relative to Fe with their CE model, [Cr/Fe]≈ -1 at [Fe/H]$= -4$. We suggest, however, that the Cr/Fe deficit obtained by François et al. (2004) is not due to inadequate yields for low- and intermediate-mass SNe II. Inspecting their Tables 1 and 2, we find very low Cr and high Fe yields (from unknown source) for stars with $20 M_\odot \leq M \leq 100 M_\odot$, which dominate Cr and Fe production at [Fe/H] ≤ -4. WW95 provide yields only for $M \leq 40 M_\odot$ models, and their Cr/Fe production ratios for solar-metallicity stars with $M > 15 M_\odot$ are supersolar. In the second case (b), we adopt the metallicity-dependent WW95 yields for Cr and Fe calculated for $Z/Z_\odot = 0, 10^{-4}, 10^{-2}, 10^{-1}, 1$, and we perform linear interpolation between these values. The third set (c) differs from the case (b) in that for $Z = 0$ we use the yields of Heger & Woosley (2008), computed for metal-free progenitors.

The [Cr/Fe] versus [Fe/H] relations computed with the chemical evolution models (a) to (c) are compared with NLTE and LTE abundance ratios in Fig. 6. The theoretical [Cr/Fe] ratios are normalized to the solar abundances of Cr and Fe, predicted by each of the models. The Cr abundance in the ISM at the solar system formation computed with the model (a) is 5.61 dex, whereas the models (b) and (c) predict $\log \varepsilon_{\rm Cr,\odot} = 5.68$ dex. The high abundance of Cr in the models (b) and (c) is compensated by a higher Fe abundance $\log \varepsilon_{\rm Fe,\odot} = 7.53$. The [Cr/Fe] trend based on LTE abundances derived from Cr I lines is qualitatively reproduced by the model (a) with adjusted WW95 yields. [Cr/Fe] decreases with metallicity. This result is expected because our LTE abundances generally agree with the spectroscopic abundances in metal-poor stars used by François et al. (2004) to calibrate SN yields in their model. The flat [Cr/Fe] trend based on NLTE abundances of Cr is well followed by the model (b). Deviations of [Cr/Fe] from zero are due to mass and metallicity-dependence of yields in the WW95 models. The Cr/Fe production ratios are supersolar for more massive stars, $M \geq 18 M_{\odot}$, with $Z/Z_{\odot} = 0.01, 0.1, 1$. However, the IMF-integrated Cr/Fe production ratios are subsolar for SNe II with $Z = 0.01$ and $Z = 0.1$ that is reflected in declining [Cr/Fe] for metallicities $-2 <$ [Fe/H] < -1. At [Fe/H] > -1, [Cr/Fe] rises again due to supersolar Cr/Fe production from exploded massive stars with initial solar metallicity, $Z = Z_{\odot}$. The total solar Cr abundance is attained due to dominant contribution ($\sim$ 60%) of SNe Ia to production of this element. We obtain similar results using the new nucleosynthesis yields of Heger & Woosley (2008) for metal-free stars, model (c) in Fig. 6. The difference with model (b) can be seen only at very low metallicity, [Fe/H] < -3.

Evolutionary curves for [Cr/Fe], which are similar to the models (b) and (c), were calculated by Timmes et al. (1995); Samland (1998); Argast et al. (2000); Goswami & Prantzos (2000); Kobayashi et al. (2006). However, good agreement between our NLTE [Cr/Fe] trend and predictions of different theoretical GCE models does not allow us to constrain the latter. The reason is that different studies adopt different prescriptions for stellar nucleosynthesis, mixing in the ISM, recipes for inflow and outflow, IMF, etc. We are not aware of any complete systematic study in the literature, focusing on the effect of these and other parameters on evolution of elemental abundance ratios. Studies analogous to that of Romano et al. (2005), who investigated the effect of initial mass function and stellar lifetimes, are highly desirable.

7. Conclusions

The atomic level populations of Cr in the atmospheres of late-type stars are very sensitive to the non-local UV radiation field, which drives them away from the LTE distribution given by Saha-Boltzmann statistics. Using 1D static model atmospheres, we find strong NLTE effects for the minority ion Cr I, they are related to overionization from the low-excitation odd Cr I levels with large quantum-mechanical photoionization cross-sections. The NLTE abundance corrections to Cr I lines are positive and increase with decreasing model metallicity and gravity. The number densities of excited states in Cr II are also modified by non-equilibrium excitation processes, but the effect on abundances is negligible for dwarfs and subgiants analyzed in this work.

Ionization equilibrium of Cr for the Sun and the metal-poor stars is satisfied, if we allow for extreme NLTE effects in Cr I by neglecting inelastic collisions with H I in statistical equilibrium calculations. For the Sun, the NLTE Cr abundance is 5.74 ± 0.04 dex, it is 0.05 dex lower than that computed from Cr II lines. Both values disagree with the Cr abundance in C I meteorites, 5.63 ± 0.01 dex (this value was taken from Lodders et al. (2009) and was renormalized to the photospheric Si abundance of Shi et al. (2008)). A few Cr I and Cr II lines give systematically higher abundances. Since these lines are sensitive to microturbulence parameter, the abundance anomaly most likely reflects the shortcomings of our 1D model atmospheres. Line formation calculations with 3D hydrodynamical models are necessary to confirm this.

The NLTE Cr I-based abundances in metal-poor stars are systematically larger than that computed under LTE approach. The difference of 0.2 – 0.4 dex is due to substantial overionization of Cr I at low metallicity. The LTE abundances determined in this work using Cr I lines are consistent with other LTE studies (Johnson 2002; Cayrel et al. 2004; Cohen et al. 2004; Lai et al. 2008; Bonifacio et al. 2009), confirming that declining [Cr/Fe] with metallicity is an artifact of LTE assumption in line formation calculations. The mean NLTE [Cr/Fe] ratio in stars with subsolar metallicity computed from Cr I lines is $\langle$[Cr/Fe]$\rangle = 0$ with the standard deviation $\sigma = 0.06$ dex. Using the Cr II lines, we derive $\langle$[Cr/Fe]$\rangle = -0.05 \pm 0.04$ dex. The finding that [Cr/Fe] remains constant down to lowest metallicities is consistent with nucleosynthesis theory, which predicts that Cr and Fe are co-produced in explosive Si-burning in supernovae.

The NLTE [Cr/Fe] trend with [Fe/H] is reproduced by most of the Galactic chemical evolution models, without the need to invoke peculiar conditions in the ISM or to adjust theoretical stellar yields. Our theoretical evolution of [Cr/Fe] in the solar neighborhood, computed with the two-infall GCE model of Chiappini et al. (1997) with SN Ia yields from Iwamoto et al. (1999) and metallicity-dependent SN II yields from Woosley & Weaver (1995), is in agreement with the NLTE results. The model predicts that $\sim$ 60% of the total solar Cr and Fe are due to SNe Ia and the rest due to SNe II, the latter synthesize both elements in roughly solar proportions. The underproduction of Cr relative to Fe in SNe Ia is compensated by its overproduction in solar-metallicity SNe II.

Acknowledgements. Based on observations made with the European Southern Observatory telescopes (obtained from the ESO/ST-ECF Science Archive Facility) and the Calar Alto Observatory telescopes. MB thanks Dr. Aldo Serenelli for useful comments on nucleosynthesis of Cr and critical revision of the manuscript.

References

Allen, C. W. 1973, Astrophysical quantities (London: University of London, Athlone Press, 1973, 3rd ed.)
Alonso, A., Arribas, S., & Martinez-Roger, C. 1996, A&AS, 117, 227
Alonso, A., Arribas, S., & Martínez-Roger, C. 1999, A&AS, 139, 335
Anstee, S. D. & O'Mara, B. J. 1995, MNRAS, 276, 859
Argast, D., Samland, M., Gerhard, O. E., & Thielemann, F.-K. 2000, A&A, 356, 873
Asplund, M. 2005, ARA&A, 43, 481
Asplund, M., Grevesse, N., Sauval, A. J., & Scott, P. 2009, ARA&A, 47, 481
Asplund, M., Ludwig, H., Nordlund, A., & Stein, R. F. 2000, A&A, 359, 669

Bagnulo, S., Jehin, E., Ledoux, C., et al. 2003, The Messenger, 114, 10

Bai, G. S., Zhao, G., Chen, Y. Q., et al. 2004, A&A, 425, 671

Barklem, P. S., Stempels, H. C., Allende Prieto, C., et al. 2002, A&A, 385, 951

Baumueller, D., Butler, K., & Gehren, T. 1998, A&A, 338, 637

Baumueller, D. & Gehren, T. 1996, A&A, 307, 961

Belyaev, A. K. & Barklem, P. S. 2003, Phys. Rev. A, 68

Belyaev, A. K., Grosser, J., Hahne, J., & Menzel, T. 1999, Phys. Rev. A, 60, 2151

Bergemann, M. & Gehren, T. 2008, A&A, 492, 823

Bergemann, M., Pickering, J. C., & Gehren, T. 2009, MNRAS, 1703

Blackwell, D. E., Booth, A. J., Menon, S. L. R., & Petford, A. D. 1986, MNRAS, 220, 303

Blackwell, D. E., Booth, A. J., Menon, S. L. R., & Petford, A. D. 1987, A&A, 180, 229

Böhm-Vitense, E. 1958, Zeitschrift für Astrophysik, 46, 108

Bonifacio, P., Spite, M., Cayrel, R., et al. 2009, A&A, 501, 519

Botnen, A. & Carlsson, M. 1999, in Numerical Astrophysics, ed. S. Miyama, K. Tomisaka, & T. Hanawa, Astrophysics and space science library

Butler, K. & Giddings, J. 1985, Newsletter on Analysis of Astronomical Spectra, University of London, 9

Casagrande, L., Ramirez, I., Melendez, J., Bessell, M., & Asplund, M. 2010, ArXiv e-prints

Cayrel, R., Depagne, E., Spite, M., et al. 2004, A&A, 416, 1117

Chiappini, C., Matteucci, F., & Gratton, R. 1997, ApJ, 477, 765

Clayton, D. 2003, Handbook of Isotopes in the Cosmos (Cambridge University Press, Cambridge, UK)

Cohen, J. G., Christlieb, N., McWilliam, A., et al. 2004, ApJ, 612, 1107

Drawin, H. W. 1969, Zeitschrift fur Physik, 225, 470

François, P., Matteucci, F., Cayrel, R., et al. 2004, A&A, 421, 613

Fuhr, J. R., Martin, G. A., & Wiese, W. L. 1988, Atomic transition probabilities. Scandium through Manganese (New York: American Institute of Physics (AIP) and American Chemical Society)

Fuhrmann, K., Axer, M., & Gehren, T. 1993, A&A, 271, 451

Fuhrmann, K., Pfeiffer, M., Frank, C., Reetz, J., & Gehren, T. 1997, A&A, 323, 909

Gehren, T., Butler, K., Mashonkina, L., Reetz, J., & Shi, J. 2001a, A&A, 366, 981

Gehren, T., Korn, A. J., & Shi, J. 2001b, A&A, 380, 645

Gehren, T., Liang, Y. C., Shi, J. R., & Zhang, H. W.and Zhao, G. 2004, A&A, 413, 1045

Gehren, T., Shi, J. R., Zhang, H. W., Zhao, G., & Korn, A. J. 2006, A&A, 451, 1065

Goswami, A. & Prantzos, N. 2000, A&A, 359, 191

Gratton, R. G., Carretta, E., Claudi, R., Lucatello, S., & Barbieri, M. 2003, A&A, 404, 187

Gratton, R. G. & Sneden, C. 1991, A&A, 241, 501

Grupp, F. 2004, A&A, 420, 289

Heger, A. & Woosley, S. E. 2008, ArXiv e-prints

Henry, R. B. C., Cowan, J. J., & Sobeck, J. 2010, ApJ, 709, 715

Hix, W. R. & Thielemann, F. 1999, ApJ, 511, 862

Holweger, H. 1967, Zeitschrift fur Astrophysik, 65, 365

Iwamoto, K., Brachwitz, F., Nomoto, K., et al. 1999, ApJS, 125, 439

Johnson, J. A. 2002, ApJS, 139, 219

Kobayashi, C., Umeda, H., Nomoto, K., Tominaga, N., & Ohkubo, T. 2006, ApJ, 653, 1145

Kostyk, R. I. & Orlova, T. V. 1983, Astrometriia i Astrofizika, 49, 39

Kurucz, R. L. 1992, Revista Mexicana de Astronomia y Astrofisica, vol. 23, 45

Kurucz, R. L., Furenlid, I., Brault, J., & Testerman, L. 1984, Solar flux atlas from 296 to 1300 nm (National Solar Observatory Atlas, Sunspot, New Mexico: National Solar Observatory, 1984)

Lai, D. K., Bolte, M., Johnson, J. A., et al. 2008, ApJ, 681, 1524

Lodders, K., Palme, H., & Gail, H. 2009, ArXiv e-prints

Mashonkina, L., Gehren, T., Shi, J., Korn, A., & Grupp, F. 2010, in IAU Symposium, Vol. 265, IAU Symposium, ed. K. Cunha, M. Spite, & B. Barbuy, 197–200

Mashonkina, L. J. 1996, in Astronomical Society of the Pacific Conference Series, Vol. 108, M.A.S.S., Model Atmospheres and Spectrum Synthesis, ed. S. J. Adelman, F. Kupka, & W. W. Weiss, 140

Matteucci, F. & Greggio, L. 1986, A&A, 154, 279

McWilliam, A., Preston, G. W., Sneden, C., & Searle, L. 1995, AJ, 109, 2757

Menzel, D. H. & Pekeris, C. L. 1935, MNRAS, 96, 77

Nagataki, S., Hashimoto, M.-A., Sato, K., & Yamada, S. 1997, ApJ, 486, 1026

Nahar, S. N. 2009, Journal of Quantitative Spectroscopy and Radiative Transfer, 110, 2148

Nakamura, T., Umeda, H., Nomoto, K., Thielemann, F.-K., & Burrows, A. 1999, ApJ, 517, 193

Nilsson, H., Ljung, G., Lundberg, H., & Nielsen, K. E. 2006, A&A, 445, 1165

Nomoto, K., Thielemann, F., & Yokoi, K. 1984, ApJ, 286, 644

Prochaska, J. X., Naumov, S. O., Carney, B. W., McWilliam, A., & Wolfe, A. M. 2000, AJ, 120, 2513

Romano, D., Chiappini, C., Matteucci, F., & Tosi, M. 2005, A&A, 430, 491

Rutten, R. J. 2003, in Astronomical Society of the Pacific Conference Series, Vol. 288, Stellar Atmosphere Modeling, ed. I. Hubeny, D. Mihalas, & K. Werner, 99

Ryan, S. G., Norris, J. E., & Beers, T. C. 1996, ApJ, 471, 254

Samland, M. 1998, ApJ, 496, 155

Scalo, J. M. 1986, Fundamentals of Cosmic Physics, 11, 1

Shchukina, N. & Trujillo Bueno, J. 2001, ApJ, 550, 970

Shi, J. R., Gehren, T., Butler, K., Mashonkina, L. I., & Zhao, G. 2008, A&A, 486, 303

Shi, J. R., Gehren, T., Zhang, H. W., Zeng, J. L., & Zhao, G. 2007, A&A, 465, 587

Sobeck, J. S., Lawler, J. E., & Sneden, C. 2007, ApJ, 667, 1267

Steffen, M. & Holweger, H. 2002, A&A, 387, 258

Talbot, Jr., R. J. & Arnett, W. D. 1975, ApJ, 197, 551

Thielemann, F.-K., Fröhlich, C., Hirschi, R., & et al. 2007, Progress in Particle and Nuclear Physics, 59, 74

Timmes, F. X., Woosley, S. E., & Weaver, T. A. 1995, ApJS, 98, 617

Umeda, H. & Nomoto, K. 2002, ApJ, 565, 385
Umeda, H. & Nomoto, K. 2005, ApJ, 619, 427
van Regemorter, H. 1962, ApJ, 136, 906
Woosley, S. E. & Weaver, T. A. 1995, ApJS, 101, 181
Wujec, T. & Weniger, S. 1981, Journal of Quantitative Spectroscopy and Radiative Transfer, 25, 167